

Potassium Channels Control the Interaction between Active Dendritic Integration Compartments in Layer 5 Cortical Pyramidal Neurons

Mark T. Harnett,¹ Ning-Long Xu,¹ Jeffrey C. Magee,^{1,*} and Stephen R. Williams^{2,*}

¹Howard Hughes Medical Institute, Janelia Farm Research Campus, Ashburn, VA 20147, USA

²Queensland Brain Institute, The University of Queensland, Brisbane, QLD 4072, Australia

*Correspondence: mageej@janelia.hhmi.org (J.C.M.), srw@uq.edu.au (S.R.W.)

<http://dx.doi.org/10.1016/j.neuron.2013.06.005>

SUMMARY

Active dendritic synaptic integration enhances the computational power of neurons. Such nonlinear processing generates an object-localization signal in the apical dendritic tuft of layer 5B cortical pyramidal neurons during sensory-motor behavior. Here, we employ electrophysiological and optical approaches in brain slices and behaving animals to investigate how excitatory synaptic input to this distal dendritic compartment influences neuronal output. We find that active dendritic integration throughout the apical dendritic tuft is highly compartmentalized by voltage-gated potassium (K_V) channels. A high density of both transient and sustained K_V channels was observed in all apical dendritic compartments. These channels potentially regulated the interaction between apical dendritic tuft, trunk, and axosomatic integration zones to control neuronal output in vitro as well as the engagement of dendritic nonlinear processing in vivo during sensory-motor behavior. Thus, K_V channels dynamically tune the interaction between active dendritic integration compartments in layer 5B pyramidal neurons to shape behaviorally relevant neuronal computations.

INTRODUCTION

Layer 5B (L5B) pyramidal neurons are the major output neurons of the neocortex, and so represent the final site of neocortical integration. Accordingly, these neurons have an extensive dendritic arbor spanning the neocortical layers to sample multiple streams of functionally distinct excitatory synaptic input targeted to specific dendritic domains (Caulier et al., 1998; Oberlaender et al., 2012; Petreanu et al., 2009; Wimmer et al., 2010). In anesthetized and behaving animals, L5B pyramidal neurons are the most active excitatory neurons in the neocortex, responding robustly to physiologically relevant stimuli with changes in the rate and pattern of action potential (AP) output (de Kock and Sakmann, 2008; O'Connor et al., 2010). The role of active dendritic integration in shaping the AP output of L5B pyramidal neu-

rons has received considerable experimental attention, revealing that dendritic synaptic input can engage voltage-gated conductances and nonlinear excitatory synaptic mechanisms (Larkum et al., 1999, 2004; Larkum and Zhu, 2002; Schiller et al., 1997, 2000; Williams, 2005; Williams and Stuart, 2002). We have recently demonstrated that such nonlinear dendritic processing is engaged during behavior in a subset of L5B pyramidal neurons during an active whisking task, leading to the generation of large amplitude coherent Ca^{2+} signals, driven by long-lasting dendritic plateau potentials, throughout the apical dendritic tuft (Xu et al., 2012).

The apical dendritic tuft is a complex, highly branched structure made up of thin caliber dendrites exhibiting a high density of dendritic spines (Larkman, 1991) that receive long-range intracortical input originating from widespread neocortical areas (Caulier et al., 1998; Caulier and Connors, 1994; Petreanu et al., 2009). These afferents convey top-down signals such as attention, expectation, and action command (Gilbert and Sigman, 2007; Gregoriou et al., 2009; Hupe et al., 1998; Xu et al., 2012). Top-down signals to L5B pyramidal neurons are crucial for the generation of coherent apical dendritic tuft Ca^{2+} signals (Xu et al., 2012). However, the determinants of membrane excitability and the mechanism(s) by which top-down signals influence the neuronal output of L5B pyramidal neurons, as well as other classes of pyramidal neurons, remain largely unknown.

In order to address these issues, we have applied multisite whole-cell recording, high-resolution patch-based channel mapping, and optical techniques to L5B pyramidal neurons in acute brain slices, together with in vivo imaging in behaving animals. We find that voltage-gated potassium channels, expressed at high density throughout the apical dendritic tree, regulate the interaction between apical dendritic tuft, trunk, and axosomatic integration compartments, by controlling the threshold and duration of dendritic spiking. Potassium channels therefore dynamically tune the interplay between active integration compartments in pyramidal neurons to powerfully control behaviorally relevant neuronal computations.

RESULTS

Layer 5B Pyramidal Neurons Have Multiple Apical Dendritic Integration Compartments

Whole-cell recording techniques were used to study the integrative operations of the apical dendritic arbor of L5B pyramidal

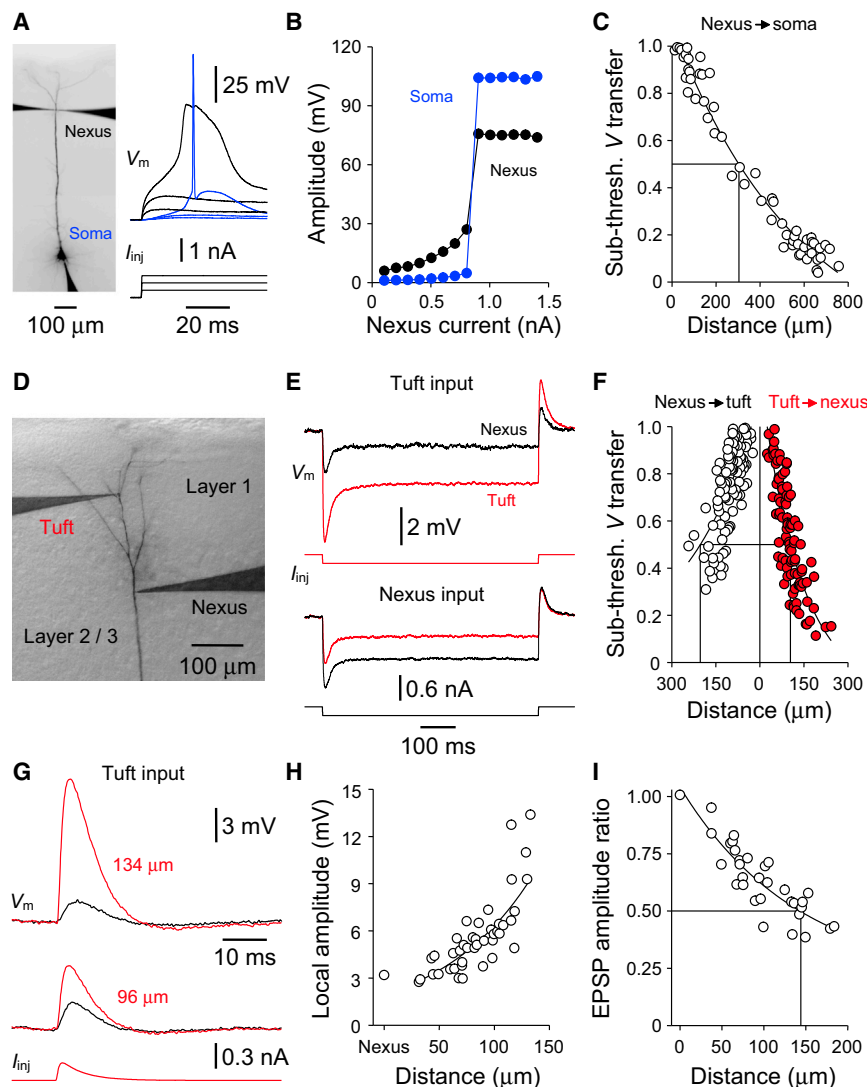


Figure 1. Voltage Compartmentalization in the Apical Dendritic Tree

(A) The injection of positive current steps at the nexus (black traces) evokes a forward propagating trunk spike that drives action potential (AP) output (blue traces). The photomicrograph shows the placement of recording electrodes.

(B) Pooled current-threshold aligned input-output relationship ($n = 61$ neurons). The peak amplitude of voltage responses at the nexus (black symbols) increases until a threshold is reached, after which a trunk spike is initiated that forward propagates to the soma to drive AP output (blue symbols). Values represent mean \pm SEM.

(C) Distance-dependent subthreshold voltage attenuation from the nexus to proximal trunk and somatic sites. Distance refers to separation between recording electrodes. The 50% attenuation point (drop line) is indicated. The curve illustrates an exponential fit to the data.

(D) Photomicrograph of the tuft of a layer 5B pyramidal neuron showing the placement of recording electrodes.

(E) Voltage attenuation between a secondary tuft dendrite (red trace, 186 μm from the nexus) and the nexus (black trace) is asymmetrical.

(F) Asymmetrical distance-dependent attenuation of subthreshold voltage responses. Distance refers to separation between recording electrodes. The 50% attenuation points (drop lines) are indicated. The curves are exponential fits to the data.

(G) Site-dependent increase in the local amplitude of simulated EPSPs at tuft sites (red traces), and their diminishing impact at the nexus (black traces).

(H) Distance-dependent increase in the local amplitude of simulated EPSPs generated at tuft sites. The curve represents an exponential fit to the data. Distance indicates recording distance from the nexus.

(I) Decremental impact of tuft EPSPs. Ratio of the peak amplitude of nexus recorded EPSPs generated at the nexus versus those generated at tuft sites. In (H) and (I), the nexus point represents the average of dual nexus recordings ($n = 5$; $<10 \mu\text{m}$ from nexus).

See also Figure S1.

neurons in acute brain slices of rat neocortex. Simultaneous whole-cell recordings from the soma and the base of the apical dendritic tuft, referred to as the nexus of the apical dendritic trunk, revealed a low-threshold site for active dendritic integration (Figure 1A). In confirmation of previous reports, a stereotyped, large amplitude, dendritic trunk spike could be evoked by the injection of suprathreshold steps of positive current at the nexus, which robustly forward propagated to the soma and axon to initiate AP firing (distance from soma = $639 \pm 9 \mu\text{m}$; $n = 61$; Figures 1A and 1B), overcoming the pronounced distance-dependent attenuation of subthreshold voltage responses as they spread from the nexus along the dendritic trunk toward the soma (current step: -200 pA , $V_{\text{proximal}}/V_{\text{nexus}}$ voltage transfer measured at peak amplitude; 50% attenuation point = $304 \mu\text{m}$; $n = 57$; Figure 1C) (Larkum and Zhu, 2002; Williams, 2004; Williams and Stuart, 2002). Simultaneous apical dendritic nexus

and trunk recordings demonstrated that apical dendritic trunk spikes were initiated in the most distal $\sim 200 \mu\text{m}$ of the apical dendritic trunk (Figure S1 available online), suggesting that this region may act as an integration site for synaptic input received in the tuft (Larkum et al., 2009; Williams and Stuart, 2002).

To delineate the constraints of such an integration scheme, we made simultaneous recordings from the thin caliber dendrites of the tuft and the nexus (Figure 1D). We found that subthreshold voltage responses attenuated as they spread from the tuft site of generation to the nexus with a 50% attenuation point of $104 \mu\text{m}$ (current step: -200 pA ; $V_{\text{nexus}}/V_{\text{tuft}}$ transfer measured at peak amplitude; $n = 96$; Figures 1D–1F). This pattern of voltage attenuation was asymmetrical, as voltage responses generated at the nexus spread with less attenuation to tuft recording sites (50% attenuation point = $203 \mu\text{m}$; Figures 1E and 1F). The characteristics of this electrical

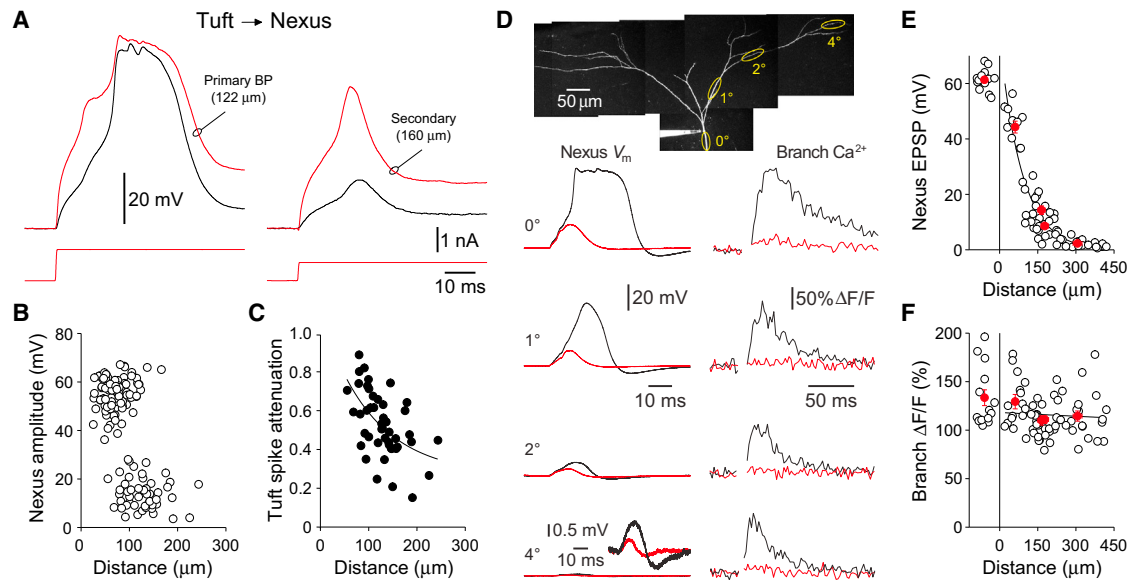


Figure 2. Compartmentalized Active Integration in the Apical Dendritic Tuft

(A) Simultaneous tuft (red) and nexus (black) recordings illustrating the generation of a complex spike at a primary tuft branch point (left) and an isolated tuft spike initiated from a secondary tuft dendrite (right).

(B) Distribution of the amplitude of spikes, measured from baseline, recorded from the nexus as a function of the site of excitation in the apical dendritic tuft. The larger amplitude cluster represents nexus generated spikes, whereas the lower amplitude events represent isolated tuft spikes.

(C) Distance-dependent attenuation of dendritic tuft spikes. Distance refers to electrode separation. The line illustrates an exponential fit to the data.

(D) Voltage responses (nexus V_m) and Ca^{2+} (Oregon Green Bapta-6F, Branch Ca^{2+}) evoked by multisite two-photon glutamate uncaging at distal apical dendritic locations (0° – 4° branch order, as indicated by photomicrograph). Black traces show suprathreshold responses evoked by increased uncaging laser intensities accompanied by large dendritic branch Ca^{2+} signals recorded from line scans close to each uncaging site. The inset shows the voltage response evoked by glutamate uncaging at the 4° tuft site at a higher magnification; note the small difference in the amplitude of voltage responses evoked by glutamate uncaging, which were sub- (red trace) and suprathreshold (black trace) for branch Ca^{2+} signaling.

(E) Distance-dependent impact of glutamate uncaging evoked voltage responses at the nexus; all responses were suprathreshold for the generation of apical dendritic branch Ca^{2+} signals. Red symbols represent data averaged by branch order (mean \pm SEM). The line illustrates an exponential fit to apical dendritic tuft data.

(F) Pooled data illustrating the uniform local branch Ca^{2+} signals evoked by suprathreshold glutamate uncaging. Red symbols represent data averaged by branch order (mean \pm SEM). The line illustrates regression analysis of apical dendritic tuft data.

See also [Figures S1](#), [S2](#), and [S3](#).

compartmentalization were further explored by the generation of simulated excitatory postsynaptic potentials (simEPSPs) at tuft sites (EPSC amplitude = 200 pA, τ_{rise} = 0.5 ms, τ_{decay} = 5 ms; n = 42). The amplitude of simEPSPs at their site of generation increased as they were generated more remotely in the tuft ([Figures 1G](#) and [1H](#)) but attenuated as they spread to the nexus (50% attenuation point = 85 μ m; not shown). Consequently, tuft-generated simEPSPs had a diminishing impact at the nexus, when directly compared with nexus-generated simEPSPs (peak amplitude: 50% attenuation = 144 μ m; area: 50% attenuation = 150 μ m; n = 32; [Figure 1I](#)). Taken together, these data indicate that the apical dendritic tuft is a highly electrically compartmentalized structure, acting to profoundly filter synaptic potentials as they spread from tuft site of generation toward the nexus and soma.

Amplification of excitatory input by the recruitment of voltage-gated ion channels (e.g., Na^+ and Ca^{2+} channels) may act to compensate for the electrical filtering properties of the dendritic tuft to enhance the salience of distal input. To explore this, we first performed dual nexus and tuft recordings, injecting positive current steps into tuft dendrites to examine their electrical excitability. At proximal sites suprathreshold current steps could

directly evoke trunk spikes (nexus to tuft time difference = 0.35 ± 0.04 ms; electrode separation = 69 ± 3 μ m; n = 57; [Figure S1](#)). In contrast, at more distal tuft sites (close to the first branch point of the tuft), positive current steps evoked regenerative spikes with a complex waveform, where a fast-rising spike, greatest in amplitude at the tuft recording site, preceded the generation of a trunk spike ([Figure 2A](#)). At even more distal secondary and tertiary dendritic tuft sites, this fast-rising spike was evoked in isolation ([Figures 2A](#) and [S1](#)). At these remote tuft recording sites, intense excitation, which drove the local membrane potential to values positive to 0 mV, typically failed to evoke trunk spikes ([Figure S2](#)). Tuft spikes therefore do not actively propagate but rather decrementally spread to the nexus ([Figures 2B](#) and [2C](#)). Tuft spikes were blocked by tetrodotoxin (n = 16; TTX, 1 μ M), allowing us to demonstrate that the local amplitude of Na^+ spikes at the site of generation in the tuft increased as recordings were made at more distal locations, but their impact at the nexus decreased ([Figure S2](#)). These data show that although active spiking mechanisms are present in the tuft, and may be recruited locally to amplify excitatory input, they cannot actively propagate toward the trunk to overcome dendritic filtering and electrical compartmentalization.

Direct current injection does not engage synaptic receptors that may provide significant regenerative current via the voltage-dependent relief of Mg^{2+} block of NMDA receptors (Branco et al., 2010; Losonczy and Magee, 2006; Schiller et al., 2000). A previous study has shown that local electrical stimulation in layer 1 of the neocortex evokes large amplitude, local NMDA receptor-dependent spikes at apical dendritic tuft sites of L5B pyramidal neurons (Larkum et al., 2009). In order to examine the impact of this form of nonlinear integration, we employed multisite two-photon glutamate uncaging to groups of spine heads while simultaneously imaging nearby local branch Ca^{2+} signals (Figure 2D). During whole-cell recording from the nexus, glutamate uncaging to a group of nearby trunk spines evoked a large amplitude trunk spike and an associated robust Ca^{2+} signal with a discrete laser power threshold (20–30 points spread over 20–30 μm , 0.2 ms dwell time, 0.1 ms move time; $n = 14$, Oregon Green BAPTA-6F, 100 μM delivered via a whole-cell recording electrode; Figure 2D). Consistent with current injection experiments, uncaging input delivered to primary tuft dendrites triggered trunk spikes within $\sim 70 \mu m$ of the nexus ($n = 11$; Figures 2D and 2E). In contrast, at higher-order tuft dendrites uncaging-evoked EPSPs (uEPSPs) were always subthreshold for the generation of trunk spikes ($n = 51$; 2° – 5° branches; Figure 2E). Notably, simultaneous imaging at all tested dendritic tuft sites revealed large amplitude local branch Ca^{2+} signals evoked in response to glutamate uncaging (Figures 2D and 2F). The specific NMDA receptor antagonist D-(–)-2-Amino-5-phosphonopentanoic acid (D-AP5) dramatically inhibited both the uEPSP and local branch Ca^{2+} signals (50 μM , $n = 5$; Figure S3). These data indicate that local spikes can be generated by spatially restricted excitatory input throughout the tuft. However, these nonlinearities could not normalize the impact of uEPSPs at the level of the nexus, with pooled data showing a dramatic distance-dependent decrement in the amplitude of suprathreshold uEPSPs recorded at the nexus (Figure 2E). The generation of local spikes at secondary and higher-order tuft sites resulted in less than a 2-fold enhancement in amplitude at the nexus, when compared with uEPSPs that were subthreshold for the generation of branch Ca^{2+} signals ($2^\circ = 1.7 \pm 0.2$, $n = 14$; $3^\circ = 1.8 \pm 0.1$, $n = 14$; $4^\circ = 1.8 \pm 0.1$, $n = 15$; $5^\circ = 1.7 \pm 0.2$, $n = 6$; Figure 2D). Consistent with this, we observed that dendritic branch Ca^{2+} signals associated with suprathreshold uEPSPs were highly compartmentalized, often failing to spread forward in the tuft past dendritic branch points (Figure S3).

Our electrophysiological and imaging data indicate that spatially localized excitatory input can trigger spikes mediated by Na^+ channels and NMDA receptors at sites throughout the apical dendritic tuft of L5B pyramidal neurons. Tuft spikes are, however, highly compartmentalized and sharply attenuate as they spread forward toward the nexus. This compartmentalization is in striking contrast to the operation of the apical dendritic tuft in behaving animals, where two-photon Ca^{2+} imaging has shown that near synchronous, global, Ca^{2+} electrogenesis is generated throughout the apical dendritic tuft of a subset of L5B pyramidal neurons during the execution of a sensory-motor behavior (Xu et al., 2012). A potential resolution of these conflicting results may be that active integration is controlled by the

recruitment of voltage-activated outward conductances in the distal apical dendritic tree.

Distribution and Properties of Potassium Channels in the Apical Dendritic Tree

In hippocampal CA1 pyramidal neurons active dendritic integration is controlled by voltage-gated potassium (K_V) channels (Cai et al., 2004; Gasparini et al., 2004; Golding et al., 1999; Hoffman et al., 1997; Losonczy et al., 2008). In contrast, a previous study has indicated a low density of K_V channels at apical dendritic trunk sites of mature L5B pyramidal neurons (Schaefer et al., 2007). However, no information is available on the distribution of K_V channels in the apical dendritic tuft of pyramidal neurons. We therefore mapped the subcellular distribution of K_V channels in L5B neurons using high-resolution outside-out patch-clamp recording techniques (Figure 3). A high density of K_V channels was found in outside-out patches excised from the soma, where ensemble K_V channel activity exhibited little inactivation during a prolonged voltage test step (holding potential -110 mV for 500 ms, test step to $+40$ mV for 400 ms; Figure 3A), consistent with previous reports (Bekkers, 2000b; Schaefer et al., 2007). In contrast, the activation properties of ensemble K_V channels excised from proximal and distal apical dendritic trunk sites were characterized by the presence of a large transient component, which rapidly decayed to a steady state (Figures 3A and S4). The total charge of ensemble K_V channel activity therefore decreased from somatic to dendritic trunk sites, consistent with a previous report (Schaefer et al., 2007). However, we found this relationship to primarily reflect the site-dependent transformation of the kinetics of ensemble K_V channel activity (Figures 3A and 3B), a feature that was not resolved by Schaefer et al. (2007) because of the temporal resolution of their recording techniques. At dendritic tuft sites, we observed ensemble K_V channel activity with kinetic properties similar to those recorded from the apical dendritic trunk (Figure 3A). Pooled data demonstrated that the amplitude of both the transient and sustained components of ensemble K_V channel activity was uniform throughout the tuft (Figures 3C and 3D) with a density of 77 ± 4 and 23 ± 2 pS μm^{-2} , respectively (assuming a patch area of $4.5 \mu m^2$ (Engel and Jonas, 2005) and reversal potential of -86 mV (Bekkers, 2000b)). Transient and sustained components were found to first activate at approximately -40 mV, with a half-maximal activation voltage of -4 and 0 mV, respectively (Figures 3E, 3F, and S4). The components of ensemble K_V channel activity could be dissociated when a brief inactivation prepulse was generated before the activation test step, fully inactivating the transient, but not the sustained, component of ensemble K_V channel activity (prepulse to -40 mV; τ_{onset} of inactivation = 5.8 ± 0.3 ms; Figures 3A and 3G). Furthermore, the transient component was fully inactivated by a long-duration prepulse to -10 mV (500 ms), whereas the sustained component was only partially inactivated ($49.7 \pm 8\%$; $n = 10$; Figure S4). These data suggest that the transient component is mediated by an I_{A-like} K_V conductance (Bekkers, 2000b; Hoffman et al., 1997).

Pharmacological analysis revealed that both transient and sustained components were significantly reduced by the application of the K_V channel blockers quinidine (25 μM) and barium

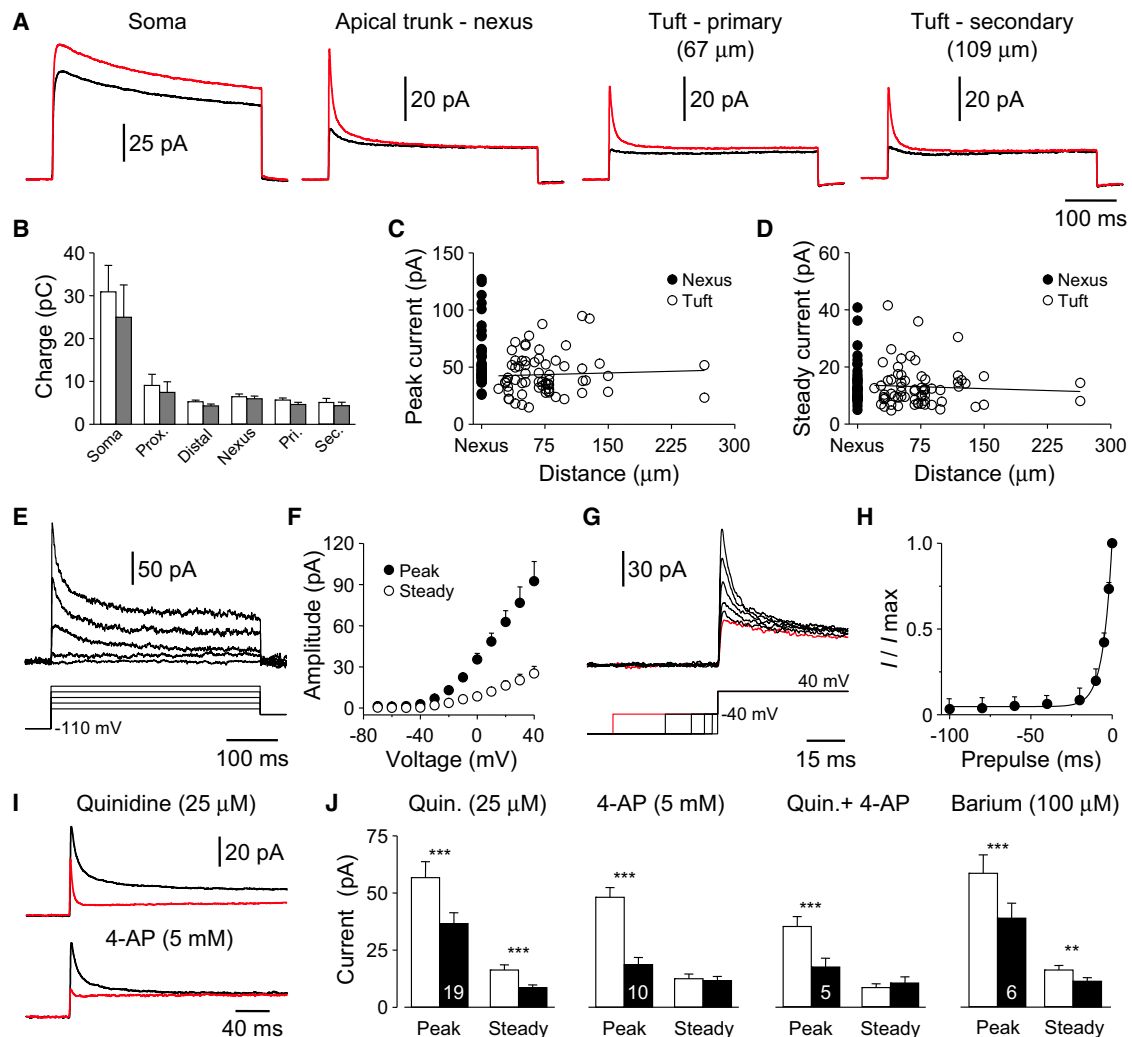


Figure 3. Density and Properties of Potassium Channels in the Apical Dendritic Tuft

(A) Averages of ensemble K_V channel activity recorded from outside-out patches excised from the indicated locations in response to a standard test step to +40 mV (red traces). The black traces illustrate average responses from the same patches when a 50 ms prepulse to -40 mV preceded the activation step. (B) Summary of the charge of ensemble K_V channel activity recorded from somatodendritic sites (open bars: activation step; gray bars: with prepulse). (C and D) Amplitude of ensemble K_V channel activity excised from the nexus of the apical dendritic trunk and tuft sites measured at peak (C) and steady state (D). Lines represent the results of linear regression. (E) Current responses (upper traces) evoked by an incremental series of positive voltage steps (lower traces) at a secondary apical dendritic tuft site (128 μ m from the nexus). (F) Pooled current-voltage relationship measured at peak (black symbols) and steady state (open symbols) from $n = 10$ patches excised from the nexus and apical dendritic tuft. (G) Inactivation of current responses (upper traces) evoked by voltage steps to +40 mV preceded (0–40 ms) by prepulses to -40 mV (lower traces), recorded from a patch excised from the apical dendritic trunk nexus. (H) Time dependence of onset of inactivation. I/I_{max} was calculated following the subtraction of steady-state current. The line is an exponential fit to the data ($n = 11$ patches from nexus and tuft sites). (I) Representative patches illustrating inhibition produced by quinidine (25 μ M; upper red trace) and 4-aminopyridine (4-AP 5 mM, lower red trace). (J) Summary of the effects of the indicated K_V channel blockers on the peak and steady-state amplitude of ensemble K_V currents excised from the nexus and apical dendritic tuft sites. The Quin. + 4-AP condition refers to the addition of 4-AP following exposure to quinidine.

** $p < 0.01$; *** $p < 0.001$. Pooled data are shown as mean \pm SEM. See also Figure S4.

(100 μ M) (total charge: control: 7.4 ± 1.1 pC, quinidine: 3.1 ± 0.5 pC, $n = 19$; control: 7.3 ± 1.2 pC, barium: 4.9 ± 0.8 pC, $n = 6$; Figures 3I and 3J). In contrast, the transient component was selectively reduced by the I_A channel blocker 4-aminopyridine (4-AP,

5 mM; Figures 3I and 3J) (Kornegreen and Sakmann, 2000). Inhibition of the transient component by quinidine was accompanied by an acceleration of time course, suggesting a mechanism of open channel blockade (half-width: control: 17.0 ± 2.5 ms,

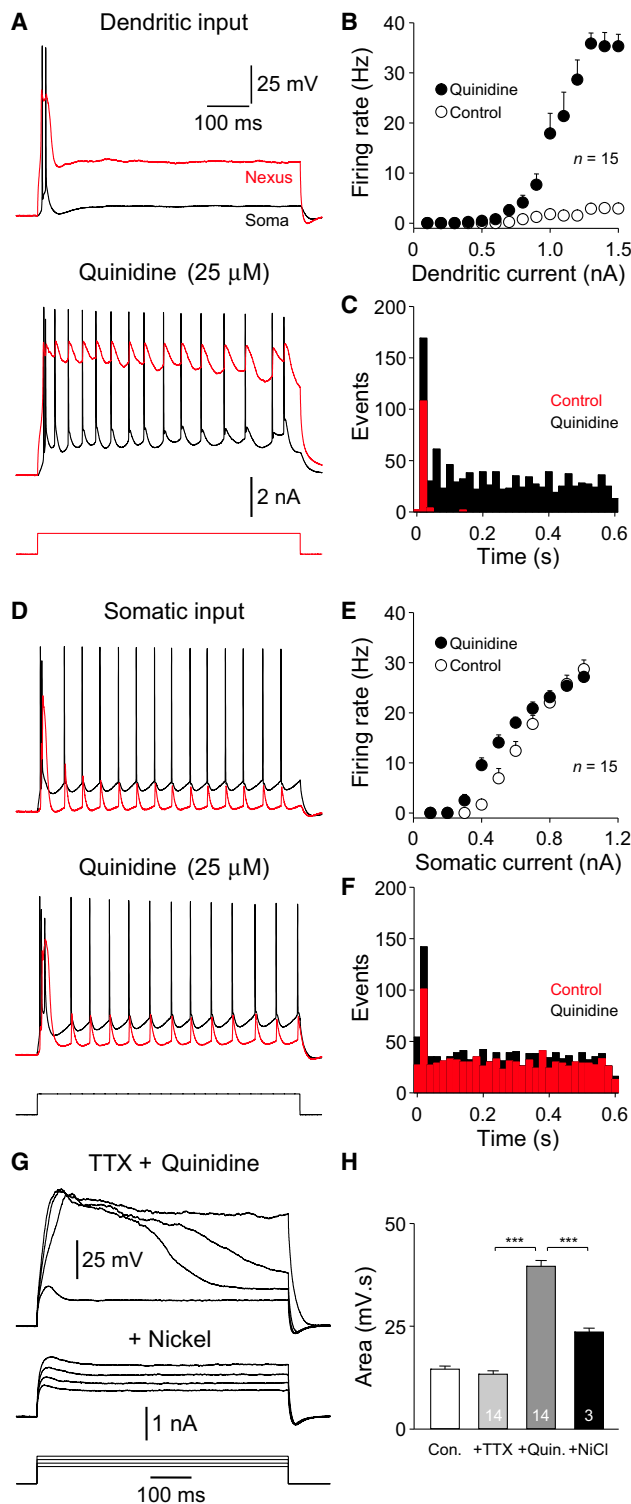


Figure 4. Potassium Channels Control Apical Dendritic Excitability
(A) Quinidine enhances axonal action potential (AP) firing evoked by apical dendritic nexus current steps. Simultaneous somatic (black) and apical dendritic nexus (red) recording.
(B) Pooled nexus current-AP output relationship under control (open symbols) and in quinidine (filled symbols). Firing rate is the number of APs per second.

quinidine: 3.5 ± 0.3 ms; charge over the first 20 ms: control: 0.70 ± 0.1 pC, quinidine: 0.23 ± 0.04 pC, $n = 19$), consistent with the reported actions of quinidine on I_A and delayed rectifier (I_{KD}) type K_V channels (Imaizumi and Giles, 1987; Yue et al., 2000). These data reveal that I_A - and I_{KD} -type K_V channels are distributed throughout the apical dendritic trunk and tuft of L5B pyramidal neurons.

Selective Control of Dendritic Integration by Potassium Channels

To determine the role of I_A - and I_{KD} -type K_V channels in regulating dendritic excitability, we first made simultaneous somatic and apical dendritic nexus recordings and constructed input-output relationship for each compartment under control and in the presence of K_V channel blockers (distance from soma = 638 ± 16 μ m; $n = 26$; Figure 4). Quinidine (25 μ M) converted transient trunk spikes into long-duration plateau potentials that drove repetitive axonal AP firing (Figures 4A–4C). In contrast, quinidine did not change the pattern of AP firing evoked by somatic excitation, or the amplitude and time course of somatically recorded APs (somatic AP half-width: control = 0.56 ± 0.01 ms; quinidine = 0.57 ± 0.01 ms; Figures 4D–4F and S5). This selective control of apical dendritic excitability was also observed with barium (50 μ M; nexus-evoked firing rate [1.4 nA]: control 3.8 ± 0.5 Hz, barium 22.3 ± 3.1 Hz; soma-evoked firing rate [1.0 nA]: control 30.0 ± 4.0 Hz, barium 28.5 ± 3.8 Hz; $n = 11$; Figure S6). These channel blockers, however, did not alter the dendritic resting membrane potential, apparent input resistance or I_H -mediated time-dependent rectification (Table S1). When taken together with the lack of effects on APs (Figure S5), these data suggest that, at the concentrations used, quinidine and barium act specifically to block K_V channels. Previous work has shown that apical dendritic trunk spikes in L5B pyramidal neurons are mediated by the regenerative recruitment of Na^+ and Ca^{2+} channels (Atkinson and Williams, 2009; Kim and Connors, 1993; Larkum and Zhu, 2002; Schiller et al., 1997). We observed that long-duration apical dendritic plateau potentials were readily generated in quinidine in the presence of the Na^+ channel blocker TTX but were abolished by the coapplication of the broad-spectrum Ca^{2+} channel antagonist nickel (250 μ M; Figures 4G and 4H). Potassium channels, therefore, powerfully control Ca^{2+} electrogenesis in the apical dendritic tree.

(C) Peristimulus time histogram of AP firing evoked by apical dendritic current under control (red) and in quinidine (black), constructed across the entire current-discharge relationship ($n = 15$ neurons).

(D) Quinidine does not alter AP firing evoked by somatic current steps. Same neuron as shown in (A).

(E) Pooled somatic current-generated current-AP output relationship under control and in quinidine.

(F) Pooled somatic current-evoked peristimulus time histogram of AP firing ($n = 15$ neurons).

(G) Apical dendritic nexus plateau potentials generated in the presence of tetrodotoxin (TTX; 1 μ M) and quinidine (25 μ M) are blocked by the Ca^{2+} channel antagonist nickel (NiCl; 250 μ M).

(H) Area of apical dendritic voltage responses evoked by a uniform input current under control and the indicated conditions. *** $p < 0.001$.

Pooled data are shown as mean \pm SEM. See also Table S1 and Figures S5 and S6.

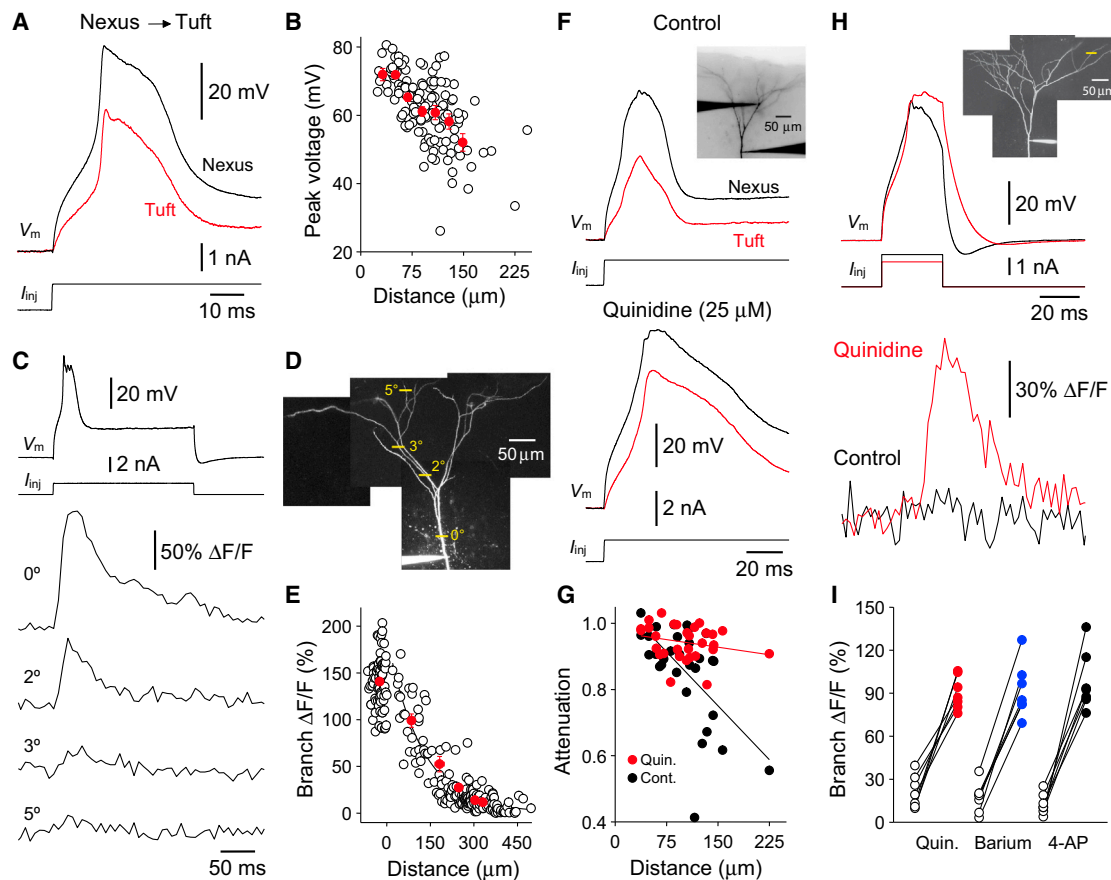
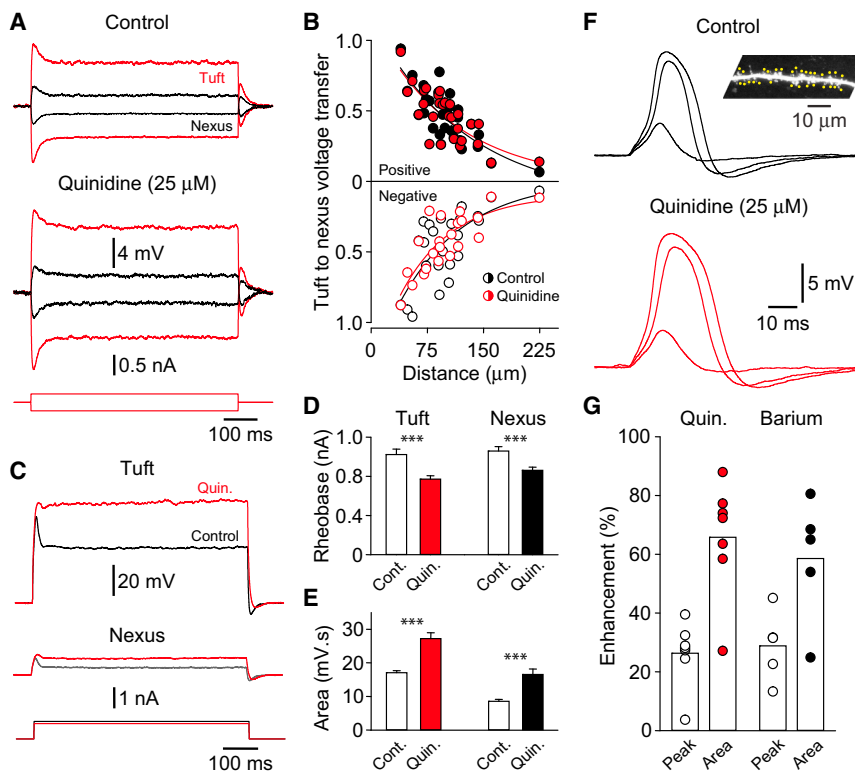


Figure 5. Potassium Channels Control the Spread of Dendritic Trunk Spikes into the Apical Dendritic Tuft

(A) Decremental spread of a nexus-evoked apical dendritic trunk spike (black) to a secondary dendritic apical tuft recording site (190 μm from the nexus, red). (B) Pooled data illustrating attenuation of the amplitude of dendritic trunk spikes as they invade the apical dendritic tuft. The red symbols illustrate data points pooled in 20 μm bins (mean \pm SEM). (C) Representative example of the distance-dependent attenuation of dendritic spike invasion into the apical dendritic tuft revealed by Ca^{2+} imaging (Oregon Green Bapta-6F). (D) Reconstruction of the apical dendritic arbor of the neuron shown in (C); the position of line scans is indicated. (E) Distance-dependent attenuation of apical dendritic trunk spike evoked Ca^{2+} signals in the apical dendritic tuft. Red symbols indicate data pooled by dendritic branch order (mean \pm SEM). The line illustrates an exponential fit. (F) The decremental spread of apical dendritic trunk spikes (black) into the apical dendritic tuft (red) is transformed by quinidine (25 μM). The inset photomicrograph shows the placement of recording electrodes. (G) Distance-dependent attenuation of dendritic trunk spikes under control (black symbols) and in quinidine (red symbols). (H) K_V channels control the invasion of dendritic trunk spikes into distal apical tuft dendrites. Simultaneous voltage recording (V_m) and terminal apical dendritic tuft Ca^{2+} imaging under control and in quinidine (25 μM , red traces). The inset photomicrograph shows the location of line scans. (I) Summary of terminal apical dendritic tuft Ca^{2+} signals under control and in the presence of the indicated K_V channel blockers (quinidine [25 μM], barium [20–50 μM], 4-aminopyridine [3 mM]). See also Figure S7.

Because our results indicate that K_V channels regulate apical trunk dendritic excitability and its control of neuronal output, we next explored how these channels influence the excitability of the apical dendritic tuft. Under control conditions, simultaneous whole-cell recording and Ca^{2+} imaging demonstrated that trunk spikes evoked by nexus current injection decrementally invaded the tuft, progressively decreasing in peak amplitude as they spread to more distal recording sites ($n = 137$; Figures 5A and 5B) and failing to evoke measurable Ca^{2+} signals at higher-order tuft sites (Oregon Green BAPTA-6F, 100 μM ; 50% attenuation point = 104 μm ; nexus = $140\% \pm 3\% \Delta\text{F}/\text{F}$, $n = 93$; fourth- to

fifth-order dendritic tuft sites = $13\% \pm 1\% \Delta\text{F}/\text{F}$, $n = 108$ branches; Figures 5C–5E). The blockade of K_V channels transformed this decremental pattern of trunk spike invasion (Figures 5F–5I). Direct electrical recording revealed that K_V channel blockade decreased the threshold current required to initiate apical dendritic trunk spikes and allowed these spikes to propagate with little decrement into the tuft (25 μM quinidine; $n = 30$; Figures 5F, 5G, and 5D). Furthermore, quinidine (25 μM), barium (20–50 μM), and the I_A channel blocker 4-AP (3 mM) dramatically enhanced trunk spike invasion into terminal tuft branches as assessed by Ca^{2+} imaging (3°–5° branches; distance from



(G) Summary of the effects of quinidine (25 μ M) and barium (20–50 μ M) on uncaging-evoked local tuft spikes recorded at the nexus. Enhancement was quantified for EPSPs with characteristic NMDA receptor-mediated regenerative voltage profiles and suprathreshold branch Ca^{2+} signals before bath application of pharmacological agents.

nexus = $313 \pm 14 \mu\text{m}$; Figures 5H and 5I). In this set of experiments, we carefully adjusted the amplitude and/or time course of positive current steps used to evoke dendritic trunk spikes, to generate spikes of amplitude, duration, and Ca^{2+} signaling similar to those recorded under control conditions at the nexus site of generation (Figure S7).

We next explored how K_V channels shape the forward propagation of voltage from tuft sites to the nexus. Quinidine (25 μM) did not alter the intense distance-dependent attenuation of subthreshold voltage responses in the tuft ($n = 30$; Figures 6A and 6B). In contrast, quinidine reduced the threshold current required for the initiation of both tuft and trunk spikes (Figures 6C and 6D) and converted short-duration tuft-generated Na^+ spikes into sustained local plateau potentials (Figures 6C and 6E). Similarly, quinidine and barium (50 μM) significantly enhanced both the peak amplitude and area of tuft spikes generated by two-photon glutamate uncaging recorded at the nexus (quinidine: $349 \pm 27 \mu\text{m}$ from nexus, $n = 7$; barium: $197 \pm 39 \mu\text{m}$, $n = 5$; Figures 6F and 6G). Taken together, these data indicate that K_V channels regulate the spread of tuft regenerative activity.

Potassium Channels Govern Interactions between Integration Compartments

Interactions between active integration compartments in pyramidal neurons facilitate correlation-based neuronal computations (Larkum et al., 2004, 1999; Takahashi and Magee, 2009; Williams,

2005), which we have shown to be exploited in L5B pyramidal neurons during behavior to produce an object localization signal (Xu et al., 2012). To investigate how K_V channels shape such interactive integration, we paired patterns of ongoing AP firing in L5B pyramidal neurons, evoked by injection of barrages of simulated EPSCs at the soma (Williams, 2005), with subthreshold apical dendritic trunk depolarization (also generated by simEPSCs; Figure 7A). Under control conditions the rate of AP firing was progressively increased by barrages of dendritic simEPSCs of increasing frequency, due to the recruitment of dendritic trunk electrogenesis (Larkum et al., 2004, 1999; Williams, 2005) (Figures 7A–7C). Quinidine (25 μM) did not alter the rate or pattern of somatically generated AP firing (control: $8.70 \pm 0.09 \text{ Hz}$; quinidine: $8.99 \pm 0.19 \text{ Hz}$, $n = 10$) but did significantly enhance the interaction between axosomatic and dendritic trunk integration compartments by recruiting sustained trunk electrogenesis, which enhanced AP output (Figures 7A–7C). We extended this analysis to the tuft, where subthreshold tuft depolarization has been shown to increase the amplitude and time course of spontaneously occurring small amplitude complex spike waveforms or back spreading trunk spikes (Xu et al., 2012). During simultaneous tuft and nexus recording quinidine (25 μM) greatly enhanced the interaction between subthreshold tuft depolarization and trunk spikes, leading to the generation of long-duration tuft plateau potentials that were manifest for the duration of the tuft excitatory input. These plateau potentials then spread to

Figure 6. Potassium Channels Control Apical Dendritic Tuft Spikes

(A) Pronounced tuft to nexus attenuation of subthreshold voltage responses evoked by positive and negative current steps at the tuft recording site is not perturbed by the blockade of K_V channels (quinidine 25 μM). Tuft recording (red traces, 143 μm from the nexus). (B) Distance-dependent attenuation of voltage signals evoked by positive and negative tuft current steps under control (black) and in quinidine (red). The lines illustrate exponential fits to the data. (C) The blockade of K_V channels (red, quinidine [25 μM]) enhances the amplitude and transforms the waveform of suprathreshold apical dendritic tuft voltage responses and their impact at the nexus. (D) Threshold current for the generation of regenerative activity at tuft and nexus recording sites under control and in quinidine (25 μM ; $n = 30$). *** $p < 0.001$. (E) Area of tuft and nexus voltage responses evoked by supra-threshold steps of positive current delivered to the tuft recording electrode under control conditions and in the presence of quinidine (25 μM ; $n = 30$). *** $p < 0.001$. Pooled data are shown as mean \pm SEM. (F) Quinidine (25 μM) augments the amplitude and duration of dendritic trunk nexus recorded EPSPs evoked by glutamate uncaging at a 2nd tuft branch (inset; 215 μm from the nexus). Overlain EPSPs were generated at increasing uncaging laser power.

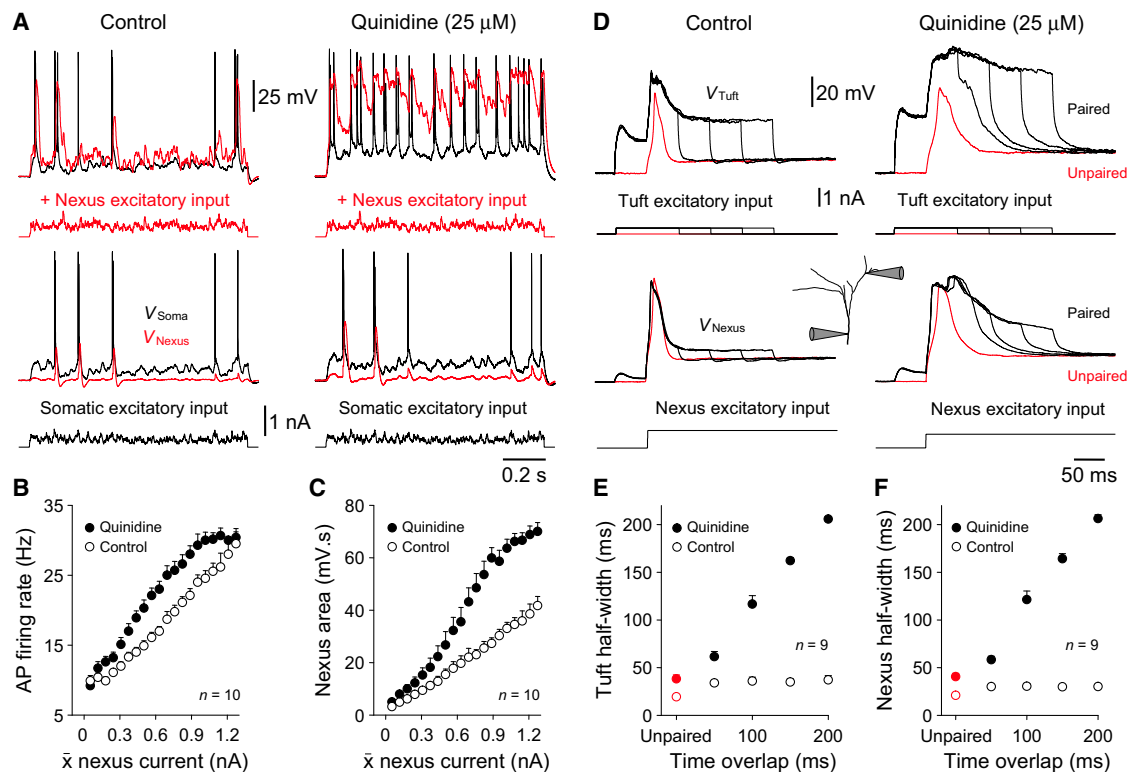


Figure 7. Apical Dendritic Potassium Channels Control Interaction between Integration Compartments

(A) Simultaneous somatic and apical dendritic nexus recordings showing the enhancement of ongoing axonal action potential (AP) firing by apical dendritic nexus simulated excitatory synaptic input under control (left traces) and in the presence of quinidine (right traces). Note the generation of large amplitude apical dendritic electrogenesis in quinidine and the enhancement of neuronal output.

(B) Summary of the enhancement of AP firing by dendritic excitation under control and in quinidine.

(C) Augmentation of dendritic electrogenesis produced by quinidine.

(D) Pairing of subthreshold apical dendritic tuft excitatory input (upper traces) with apical dendritic nexus-evoked trunk spikes (lower traces) under control and in quinidine. Red and black traces illustrate the unpaired and paired conditions, respectively. Note the prolongation of the tuft and nexus voltage responses in quinidine. The inset shows the placement of tuft (1,089 μ m from soma) and trunk (850 μ m) recording electrodes on a line reconstruction of the apical dendritic tuft.

(E and F) Enhancement of the duration of apical dendritic tuft (E) and nexus (F) electrogenesis produced by quinidine.

Pooled data are shown as mean \pm SEM.

the nexus to extend the time course of trunk spikes (average distance from nexus = 127 ± 16 μ m; $n = 9$; Figures 7D–7F).

Barium Augments Active Dendritic Integration during Behavior

The above data suggest that the regulation of K_V channel activity in the apical dendritic tuft should influence the interaction between active integration compartments in L5B pyramidal neurons during sensory-motor behavior (Xu et al., 2012). To test this, we virally expressed the Ca^{2+} indicator GCaMP3 in deep layers of the primary somatosensory vibrissa cortex of mice and subsequently performed two-photon Ca^{2+} imaging of tuft dendrites while mice performed an active whisking task (see Experimental Procedures for details; Figures 8A and 8B). Large amplitude Ca^{2+} signals were recorded from regions of interest throughout the apical dendritic tuft of a sparse subset of neurons in response to active facial whisker-object contact (Figures 8C and 8D). We have previously shown that such signals are formed by the integration of intracolumnar and long-range motor inputs

in morphologically identified murine L5B neurons, which possess apical dendritic tuft electrophysiological properties indistinguishable from those of the rat (Xu et al., 2012). The local application of barium (400 μ M) to the surface of the neocortex through an opening in the imaging window significantly and reversibly increased the occurrence, amplitude, and area of Ca^{2+} signals evoked by whisker-object contact ($n = 3$ animals; $n = 70$ imaging regions of interest [ROIs]; Figures 8C–8F and S8). Notably, barium increased the total area of Ca^{2+} signals generated per behavioral trial in 68 of 70 imaging ROI, an effect that was fully reversible (control = 4.4 ± 0.4 $\Delta F/F.s$; barium = 10.1 ± 0.7 $\Delta F/F.s$; $p < 0.001$; wash = 5.6 ± 0.4 $\Delta F/F.s$; not statistically different from control; Figures 8G and S9). In contrast, barium did not alter basal levels of fluorescence, the characteristics of whisker movement or task performance (Figures 8H–8J). As whisker movement is, in part, controlled by the somatosensory vibrissa neocortex (Matyas et al., 2010), these results suggest that the local application of barium does not globally alter excitability. The enhancement of behaviorally engaged dendritic

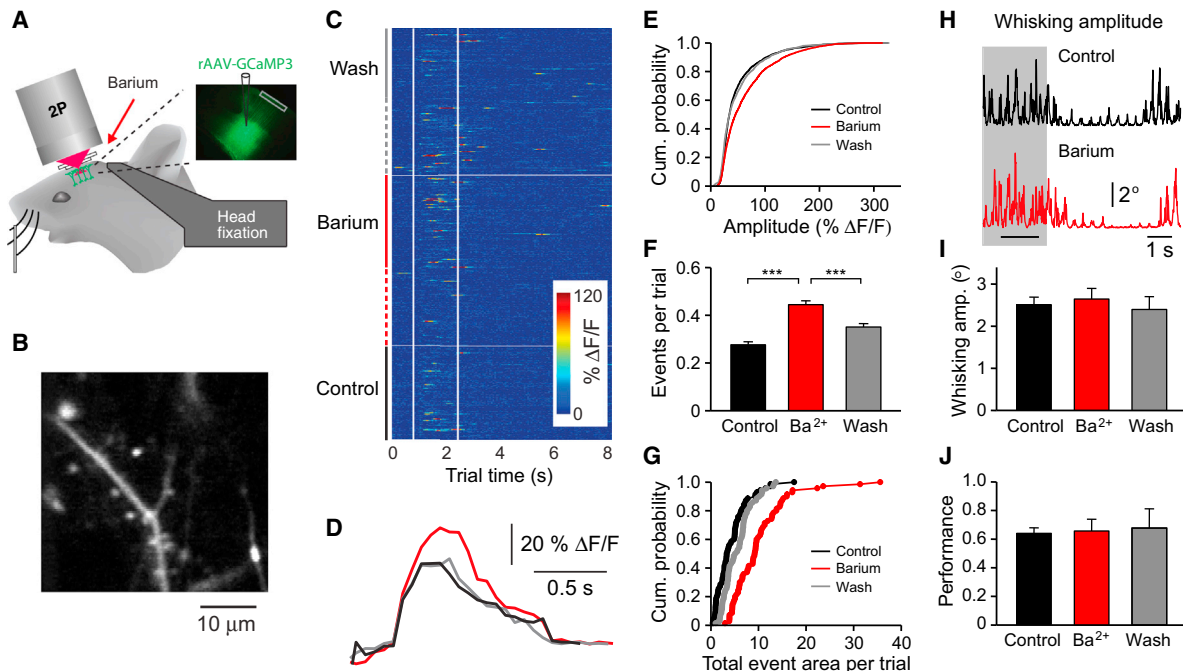


Figure 8. Potassium Channels Control Dendritic Integration during Behavior

(A) Schematic diagram of the behavioral experimental setup.
 (B) Example image of a portion of an apical dendritic tuft in a GCaMP3-infected neuron.
 (C) Color raster plot of Ca^{2+} signals recorded from an apical dendritic tuft region of interest during behavioral trials, where each row represents one behavioral trial. The vertical white lines indicate the period of object presentation. Vertical lines on the left indicate the conditions: control (black), barium (400 μM , red), and wash (gray); solid lines indicate steady-state conditions used for quantification.
 (D) Averaged traces of Ca^{2+} events detected from trials in (C).
 (E) Cumulative probability distribution of the amplitude of Ca^{2+} events under the indicated conditions.
 (F) Number of detected Ca^{2+} events per trial under the indicated conditions. *** $p < 0.001$.
 (G) Cumulative probability distribution of the total area of Ca^{2+} events per trial under the indicated conditions. Each point represents an imaging region of interest.
 (H) Barium does not change the characteristics of whisker movement. The shaded box indicates the time period used for analysis and the horizontal black bar the period of object presentation.
 (I) Summary of whisking amplitude measured over the time period indicated in (H).
 (J) Barium does not alter behavioral performance. Performance represents the fraction of correct licking responses. Pooled data are shown as mean \pm SEM. See also Figures S8 and S9.

tuft Ca^{2+} signals in L5B pyramidal neurons by barium therefore closely parallels the control of apical dendritic excitability by K_V channels in brain-slice experiments. We however cannot rule out the possibility that barium has additional pre- and/or post-synaptic actions in vivo.

A Multilayered Interactive Integration Scheme

As the availability of apical dendritic K_V channels is decreased by depolarization due to the pronounced time- and voltage-dependent inactivation of the $\text{I}_{A\text{-like}}$ component, we reasoned that the interaction between integration compartments might be strongly engaged when excitatory input is distributed throughout the apical dendritic arbor. To test this experimentally, we made triple whole-cell patch recordings from the soma, nexus, and tuft of L5B pyramidal neurons in brain slices (nexus = $685 \pm 13 \mu\text{m}$, tuft = $817 \pm 21 \mu\text{m}$ from soma; $n = 8$; Figure 9A). The rate and pattern of AP firing evoked by somatic current injection was broadly unaffected by the pairing of either subthreshold trunk or tuft excitatory input (Figures 9A and 9C). In contrast, coinci-

dent trunk and tuft excitatory input powerfully engaged dendritic electrogenesis, leading to the generation of repeated large amplitude plateau potentials at both distal recording sites, which transformed the rate and pattern of neuronal output by promoting the generation of high-frequency burst firing (Figures 9A–9C). Triple whole-cell recordings from proximal trunk, nexus, and tuft sites revealed the duration of apical dendritic tuft plateau potentials was tightly controlled by the level of tuft excitatory input (proximal trunk = $371 \pm 28 \mu\text{m}$, nexus = $808 \pm 25 \mu\text{m}$, tuft = $939 \pm 26 \mu\text{m}$ from soma; $n = 6$; Figure 9D). Together, these data directly demonstrate that apical dendritic tuft excitatory input can powerfully control the neuronal output of L5B pyramidal neurons through the engagement of interactive integration.

DISCUSSION

Excitatory synapses are distributed throughout the complex dendritic tree of L5B pyramidal neurons (Larkman, 1991). The apical dendritic tuft, morphologically and electrotonically the

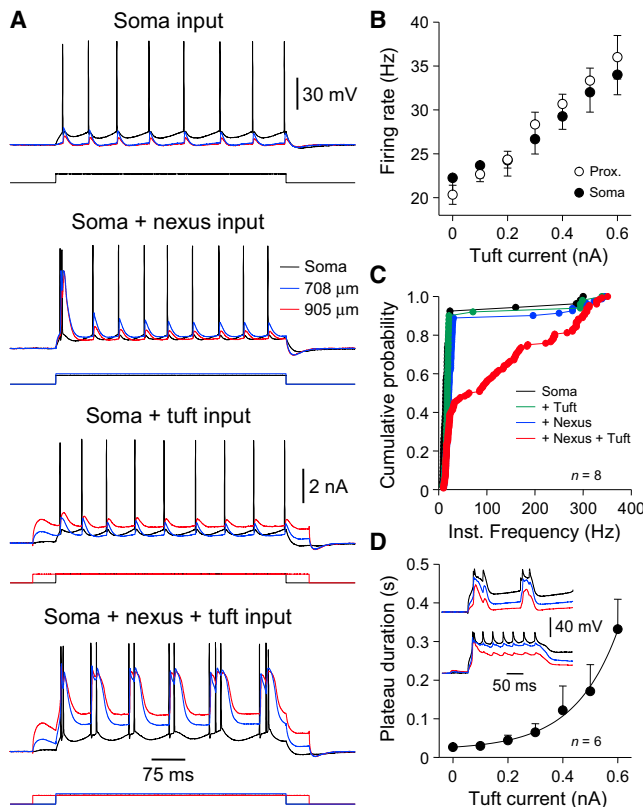


Figure 9. Multilayered Interactive Integration

(A) Simultaneous somatic (black traces), apical dendritic trunk (blue traces), and tuft (red traces) recordings illustrate the transformation of neuronal output, and the generation of apical dendritic plateau potentials, by the concerted activation of integration compartments.

(B) Control of the rate of axonal action potential (AP) firing by apical dendritic tuft excitatory input (tuft current) when paired with apical dendritic nexus and somatic (filled symbols, $n = 8$ neurons), or proximal apical dendritic trunk (open symbols, $n = 6$ neurons) excitatory input.

(C) Cumulative probability distribution of instantaneous AP firing frequency, driven by steps of positive current delivered to the soma (black symbols, 0.64 ± 0.08 nA), the soma and the apical dendritic tuft (green symbols, 0.6 nA), the soma and the apical dendritic nexus (blue symbols, 0.64 ± 0.08 nA), or the concerted activation of all three compartments (red symbols).

(D) Apical dendritic excitation controls the duration of plateau potentials, when paired with proximal apical dendritic trunk, and nexus excitatory input. Data have been fit by an exponential function. The inset shows plateau potentials generated by proximal apical dendritic trunk (black traces, $375 \mu\text{m}$ from soma), and nexus (blue traces, $735 \mu\text{m}$ from soma) excitatory input (lower overlain traces; proximal input = 1.6 nA, nexus input = 0.4 nA) and when paired with apical dendritic tuft excitatory input (red traces, $933 \mu\text{m}$ from the soma, upper overlain traces, tuft input = 0.3 nA).

Pooled data are shown as mean \pm SEM.

most remote site in these neurons, receives substantial excitatory input from long-range intracortical circuits (Cauler and Connors, 1994; Petreanu et al., 2009). We have recently shown that top-down signals to L5B pyramidal neurons are crucial for the computation of an object localization signal in the somatosensory neocortex of behaving mice (Xu et al., 2012). This decisive role of top-down signals in behaviorally relevant neuronal processing is inconsistent with classical views of neuronal func-

tion, which suggest that synaptic integration occurs at the site of AP initiation following the decremental passive electrical spread of synaptic potentials from dendritic sites of generation to the axon (Rall, 1964). Dendrites of pyramidal neurons, however, are not passive but are capable of generating regenerative electrical activity (Gasparini et al., 2004; Kim and Connors, 1993; Larkum and Zhu, 2002; Losonczy and Magee, 2006; Losonczy et al., 2008; Schiller et al., 1997, 2000; Williams and Stuart, 2002). We, and others, have suggested that apical dendritic tuft excitatory input may influence neuronal output following integration at the level of the distal apical dendritic trunk, the site of a powerful spike generator (Larkum et al., 2009; Williams, 2004; Williams and Stuart, 2002). However, the biophysical mechanisms that govern this process have remained largely elusive.

Here, we report that the apical dendritic tuft is highly electrically compartmentalized, strongly filtering subthreshold voltage signals as they spread from tuft site of generation to the apical dendritic trunk. Coupled with the intense voltage attenuation experienced along the trunk to the soma, this compartmentalization severely constrains the direct influence of tuft synaptic input on axonal AP output. Furthermore, these properties suggest that tuft excitatory input provides a limited, distance-dependent drive for dendritic spike generation in the trunk. To test how the saliency of tuft excitatory input may be increased at the trunk by the recruitment of active dendritic spiking mechanisms we used direct recording as well as two-photon imaging and glutamate uncaging techniques. In an extension of a previous study (Larkum et al., 2009), we found that local spikes could be evoked by spatially restricted patterns of excitation at sites throughout the tuft. These local spikes, mediated by Na^+ channels and NMDA receptors, had a diminishing impact at the nexus when generated from increasingly remote sites in the tuft. Indeed, across the majority of the tuft, such local nonlinear integration increased the efficacy of input signals by less than 2-fold at the nexus of the apical dendrite. Regenerative integration mechanisms in the tuft therefore function to augment local excitatory synaptic input within the tuft, but their inability to actively forward propagate strongly restricts their impact on trunk spike initiation and ultimately axonal output.

The decremental spread of local spikes from thin caliber, high apparent input resistance tuft dendrites to the larger diameter dendritic trunk directly supports theoretical analysis (Vetter et al., 2001), suggesting that the trunk represents a large electrical load. However, we demonstrate that a high density of K_V channels in the apical dendritic arbor imposes an additional and unexpected strong compartmentalization on the spread of regenerative signals in these neurons. Our direct observation of a uniformly high density of both fast-activating and -inactivating $\text{I}_{A\text{-like}}$ and noninactivating $\text{I}_{K\text{D-like}}$ K_V channels throughout the apical dendritic trunk and tuft, in both outside-out and cell-attached patches (Figure S4), is inconsistent with a previous report, which described a low density of K_V conductance in the apical dendritic trunk of mature L5B pyramidal neurons using whole-cell recording techniques (Schaefer et al., 2007). This discrepancy is suggested to be related to the contrasting recording techniques used, because our findings are consistent with and extend previous work using similar techniques made from the soma and proximal apical dendritic trunk sites of

immature L5B neurons (Bekkers, 2000a; Korngreen and Sakmann, 2000).

If tuft excitatory synaptic input is isolated from the axon, and only weakly directly drives apical dendritic trunk spike initiation, how can it influence neuronal output? We demonstrate that the apical dendritic tuft can interact in a nonlinear manner with more proximal integration zones (i.e., the axon and nexus), and that K_V channels control this process. Previous findings have revealed that axosomatic and dendritic trunk integration compartments can synergistically interact in L5B pyramidal neurons (Larkum et al., 1999, 2004; Williams, 2005). Here, we show that apical dendritic K_V channels tightly control this interaction. Indeed, K_V channels also governed the interaction between subthreshold tuft excitatory input and trunk spike generation, with the pharmacological blockade of K_V channels leading to the generation of large amplitude long-duration plateau potentials in the apical dendritic arbor. As apical dendritic K_V channels exhibit highly sensitive voltage- and time-dependent inactivation properties, widespread depolarization of the apical dendritic tuft, as may occur during behavior (Xu et al., 2012), will lead to voltage-dependent K_V channel inactivation, that is augmented by the local recruitment of NMDA-receptor- and Na^+ -channel-mediated supralinearities. These effects will powerfully influence the interaction between axosomatic and apical dendritic trunk integration compartments. Consistent with this, we find that tuft Ca^{2+} signals during behavior are enhanced by pharmacological blockade of K_V channels. These observations support a multilayer integration scheme for L5B pyramidal neurons, which we tested experimentally using triple recordings. Top-down, apical tuft excitatory input was found to decisively influence the rate and pattern of AP firing evoked via coincident activation of axosomatic and apical dendritic trunk integration compartments by controlling the duration of apical dendritic plateau potentials. Therefore, trunk spikes are not a binary output mode of apical dendritic integration, but rather are analog signals, the duration of which is tuned by apical dendritic tuft excitatory input. Our direct demonstration that apical dendritic tuft input drives high-frequency AP burst firing suggests that top-down influences such as attention, expectation, and action command (Gilbert and Sigman, 2007; Gregoriou et al., 2009; Hupe et al., 1998; Xu et al., 2012) will dramatically increase the salience of L5B pyramidal neuron output at cortical and subcortical targets, due the low initial release probability and highly facilitatory nature of these synapses (Williams, 2005; Williams and Atkinson, 2007).

In summary, we report that excitatory synaptic input from columnar and long-range intracortical circuits targeted to segregated sites within the electrically distributed dendritic tree of L5B pyramidal neurons can be integrated by the nonlinear interaction between axosomatic, apical dendritic trunk, and tuft integration compartments. Dendritic voltage-gated K_V channels control this interaction. We suggest, therefore, that apical dendritic trunk and tuft K_V channels operate as a tuneable gain control for interactive integration. As K_V channels are regulated by neuromodulatory systems (Hoffman and Johnston, 1998, 1999; Nicoll et al., 1990), apical dendritic K_V channels may represent an important target for refining interactive integration in pyramidal neurons to guide behaviorally relevant neuronal computations.

EXPERIMENTAL PROCEDURES

In Vitro Slice Preparation and Simultaneous Patch-Clamp Recording

Coronal brain slices containing the somatosensory cortices were prepared from 4- to 7-week-old male Wistar rats following university and institutional guidelines using methods previously described (Williams, 2004, 2005). Slices were submerged in artificial cerebrospinal fluid (aCSF) containing (in mM): 125 NaCl, 25 $NaHCO_3$, 1.25 NaH_2PO_4 , 3 KCl, 2 or 1.3 $CaCl_2$, 1.0 $MgCl_2$, 25 glucose, and 3 Na-pyruvate at 36°C–37°C. Dual and triple whole-cell recordings were made from thick-tufted L5B pyramidal neurons with BVC-700A (Dagan) amplifiers in “bridge” mode, and the electrode capacitance was carefully compensated. Somatic pipettes had open tip resistance of 3–6 M Ω and dendritic pipettes 10–12 M Ω , when filled with (in mM): 135 K-gluconate; 7 NaCl; 10 HEPES; 10 phosphocreatine; 2 Na_2 -ATP; 0.3 Na-GTP; 2 $MgCl_2$ and 0.01 Alexa Fluor 568 or 594 (Molecular Probes) (pH 7.3–7.4; KOH). Neuronal morphology was recorded by fluorescence microscopy (QImaging). Data were excluded if the nexus recording electrode was >50 μ m from this site. The length of the apical dendritic trunk measured from structural images (soma intersection to nexus) was 749 ± 26 μ m and diameter 2.8 ± 0.1 μ m at 20 μ m from the nexus ($n = 13$). The path length of tuft dendrites was 413 ± 14 μ m and diameter between 0.8 and 2.3 μ m ($n = 40$). Tuft recordings were discarded if series resistance was >60 M Ω . Simulated EPSCs were generated as ideal current sources (τ_{rise} and τ_{decay} of 0.5 and 5 ms, respectively). Temporally uncorrelated barrages of simulated EPSCs were generated as trains of pseudorandomly occurring inputs (peak amplitude 0.1 nA) and injected at somatic and dendritic sites as previously described (Williams, 2005). Simulated EPSCs were therefore generated at somatic and dendritic sites as point current sources and not distributed conductances. Current and voltage signals were low pass filtered (DC to 10 kHz) and acquired at 30–50 kHz. Data were acquired and analyzed using AxographX software (AxographX). All drugs were dissolved in the recording aCSF and applied by bath perfusion.

Outside-out patches were excised from somatic or apical dendritic sites using pipettes of similar open tip resistance (10–12 M Ω) filled with (in mM): 130 K-gluconate; 7 NaCl; 10 HEPES; 2 Na_2 -ATP; 0.3 Na-GTP; 2 $MgCl_2$ and 5 Ethylene glycol-bis(b-aminoethylether)-N,N,N',N'-tetraacetic acid (pH 7.3–7.4; KOH). The recording aCSF was supplemented with TTX (1 μ M), 4-ethylphenylamino-1,2-dimethyl-6-methylaminopyrimidinium chloride (10 μ M) and $CdCl_2$ (100 μ M), at room temperature (26°C–26.5°C). Ensemble K_V channel activity was recorded using a Multi-clamp 700 amplifier (Molecular Devices), electrode capacitance compensated, and low-pass filtered (DC to 5 kHz). To map channel density, ensemble K_V channel activity was generated in response to a +40 mV (400 ms) test step delivered from a conditioning voltage of –110 mV (500 ms), interleaved by the repetition of four 1/15 scaled voltage pulses for on- or off-line leak subtraction, from an intrapipette holding potential of –60 mV. Measurements were made from digital averages of >20 consecutive trials. After gathering ensemble channel data, a whole-cell recording was obtained, at the same apical dendritic site, and the neuron was dialyzed with Alexa Fluor 594 to record morphology. Data were pooled for membrane patches excised from somatic (at the soma-apical dendrite intersection), proximal apical dendritic trunk (100–120 μ m from soma), distal apical dendritic trunk (100–120 μ m from the nexus), nexus (trunk sites <30 μ m from the nexus), and apical dendritic tuft sites.

In Vitro Two-Photon Imaging and Uncaging

Whole-cell current-clamp recordings, using techniques identical to those above, were made from the distal apical trunk or primary tuft dendrite of L5B pyramidal neurons in aCSF containing (in mM): 125 NaCl, 25 $NaHCO_3$, 1.25 NaH_2PO_4 , 3 KCl, 1.3 $CaCl_2$, 1.0 $MgCl_2$, 25 glucose, 3 pyruvate, and 1 ascorbate. Pipettes had an open tip resistance of 4–6 M Ω when filled with (in mM): 134 K-gluconate, 6 KCl, 10 HEPES, 4 NaCl, 0.3 $Tris_2$ GTP, 4 Mg_2 ATP, 14 phosphocreatine, and 0.05 Alexa Fluor 594 at 34°C–37°C. Two-photon imaging and glutamate uncaging was performed using a dual galvanometer-based scanning system as previously described (Losonczy and Magee, 2006). Line scans were made at high magnification with dwell times of 8–12 μ s at 150–500 Hz, three to 12 line scans were averaged for each condition. Ca^{2+} signals are expressed as $\Delta F/F$ (%) (calculated as $[(F - F_{baseline}) / F_{baseline}] \times 100$). Data were collected from dendrites that were at least 30 μ m (and up to

150 μm) below the surface of the slice that were not prematurely cut off before termination. Branches were anatomically defined as incrementing from 0° at the apical trunk. For fast, multisite glutamate uncaging, 10 mM MNI-glutamate (Tocris; dissolved in aCSF) was delivered via pressure ejection to the surface of the slice while focused 720 nm laser light was directed to 10–30 preselected points near spine heads (0.2 ms dwell time, 0.1 ms move time).

Two-Photon Calcium Imaging in Behaving Animals

All procedures were conducted according to Institutional guidelines (Janelia Farm Research Campus Institutional Animal Care and Use Committee) and have been described previously in full (Xu et al., 2012). Briefly, adult male (>P60) C57BL/6Cr mice were anesthetized with isoflurane, a craniotomy (~2 mm in diameter) made over left barrel cortex, and the dura left intact. The genetically encoded Ca^{2+} indicator GCaMP3 expressed under the human synapsin-1 promoter following infection with recombinant adenoassociated virus (serotype 2/1; produced by the University of Pennsylvania Gene Therapy Program Vector Core) was injected stereotactically to deep layers of the primary vibrissae barrel somatosensory neocortex. The craniotomy was covered with a half-moon-shaped double-layered glass coverslip, a small portion (~0.7 mm in diameter) of the craniotomy was left open and filled with silicon gel to allow pharmacological manipulation. A titanium head-post was attached to the skull. Fourteen days after virus injection and window implantation, mice began training on the go/no-go tactile detection task (Xu et al., 2012). Briefly, a vertical pole (the target object) was presented to the right side of the mouse face either within reach by the whiskers in “go” trials (licking leads to water reward) or out of reach in “no-go” trials (licking leads to timeout without water). Mice determined the location of the object using active whisking and object contact in order to respond with lick in go trials and hold licking in no-go trials. The behavioral apparatus was mounted under a custom two-photon microscope equipped with a high-speed whisker imaging system. Apical dendritic tuft activity was imaged from GCaMP3-positive apical dendrites of layer five pyramidal neurons at depths of 20–400 μm (Xu et al., 2012). Image analysis was performed as described (Xu et al., 2012). To estimate the amplitude and frequency of individual Ca^{2+} transients, we measured the peak $\Delta F/F$ of detected Ca^{2+} events. Event detection was based on combined thresholding of the amplitude (>4 SD, estimated using median absolute deviation) and rising slope (computed from a span of three frames) of $\Delta F/F$ time series from all trials of a given ROI.

SUPPLEMENTAL INFORMATION

Supplemental Information includes Supplemental Experimental Procedures, nine figures, and one table and can be found with this article online at <http://dx.doi.org/10.1016/j.neuron.2013.06.005>.

ACKNOWLEDGMENTS

We thank A. Milstein and M. Roberts for help in creating analysis tools. This work was supported by the Australian Research Council (FT100100502), the National Health and Medical Research Council (APP1004575), and the Howard Hughes Medical Institute.

Accepted: May 30, 2013
Published: August 7, 2013

REFERENCES

- Atkinson, S.E., and Williams, S.R. (2009). Postnatal development of dendritic synaptic integration in rat neocortical pyramidal neurons. *J. Neurophysiol.* 102, 735–751.
- Bekkers, J.M. (2000a). Distribution and activation of voltage-gated potassium channels in cell-attached and outside-out patches from large layer 5 cortical pyramidal neurons of the rat. *J. Physiol.* 525, 611–620.
- Bekkers, J.M. (2000b). Properties of voltage-gated potassium currents in nucleated patches from large layer 5 cortical pyramidal neurons of the rat. *J. Physiol.* 525, 593–609.
- Branco, T., Clark, B.A., and Häusser, M. (2010). Dendritic discrimination of temporal input sequences in cortical neurons. *Science* 329, 1671–1675.
- Cai, X., Liang, C.W., Muralidharan, S., Kao, J.P., Tang, C.M., and Thompson, S.M. (2004). Unique roles of SK and Kv4.2 potassium channels in dendritic integration. *Neuron* 44, 351–364.
- Cauler, L.J., and Connors, B.W. (1994). Synaptic physiology of horizontal afferents to layer I in slices of rat SI neocortex. *J. Neurosci.* 14, 751–762.
- Cauler, L.J., Clancy, B., and Connors, B.W. (1998). Backward cortical projections to primary somatosensory cortex in rats extend long horizontal axons in layer I. *J. Comp. Neurol.* 390, 297–310.
- de Kock, C.P., and Sakmann, B. (2008). High frequency action potential bursts (>100 Hz) in L2/3 and L5B thick tufted neurons in anaesthetized and awake rat primary somatosensory cortex. *J. Physiol.* 586, 3353–3364.
- Engel, D., and Jonas, P. (2005). Presynaptic action potential amplification by voltage-gated Na^+ channels in hippocampal mossy fiber boutons. *Neuron* 45, 405–417.
- Gasparini, S., Migliore, M., and Magee, J.C. (2004). On the initiation and propagation of dendritic spikes in CA1 pyramidal neurons. *J. Neurosci.* 24, 11046–11056.
- Gilbert, C.D., and Sigman, M. (2007). Brain states: top-down influences in sensory processing. *Neuron* 54, 677–696.
- Golding, N.L., Jung, H.Y., Mickus, T., and Spruston, N. (1999). Dendritic calcium spike initiation and repolarization are controlled by distinct potassium channel subtypes in CA1 pyramidal neurons. *J. Neurosci.* 19, 8789–8798.
- Gregoriou, G.G., Gotts, S.J., Zhou, H., and Desimone, R. (2009). High-frequency, long-range coupling between prefrontal and visual cortex during attention. *Science* 324, 1207–1210.
- Hoffman, D.A., and Johnston, D. (1998). Downregulation of transient K^+ channels in dendrites of hippocampal CA1 pyramidal neurons by activation of PKA and PKC. *J. Neurosci.* 18, 3521–3528.
- Hoffman, D.A., and Johnston, D. (1999). Neuromodulation of dendritic action potentials. *J. Neurophysiol.* 81, 408–411.
- Hoffman, D.A., Magee, J.C., Colbert, C.M., and Johnston, D. (1997). K^+ channel regulation of signal propagation in dendrites of hippocampal pyramidal neurons. *Nature* 387, 869–875.
- Hupe, J.M., James, A.C., Payne, B.R., Lomber, S.G., Girard, P., and Bullier, J. (1998). Cortical feedback improves discrimination between figure and background by V1, V2 and V3 neurons. *Nature* 394, 784–787.
- Imazumi, Y., and Giles, W.R. (1987). Quinidine-induced inhibition of transient outward current in cardiac muscle. *Am. J. Physiol.* 253, H704–H708.
- Kim, H.G., and Connors, B.W. (1993). Apical dendrites of the neocortex: correlation between sodium- and calcium-dependent spiking and pyramidal cell morphology. *J. Neurosci.* 13, 5301–5311.
- Korngreen, A., and Sakmann, B. (2000). Voltage-gated K^+ channels in layer 5 neocortical pyramidal neurones from young rats: subtypes and gradients. *J. Physiol.* 525, 621–639.
- Larkman, A.U. (1991). Dendritic morphology of pyramidal neurones of the visual cortex of the rat: III. Spine distributions. *J. Comp. Neurol.* 306, 332–343.
- Larkum, M.E., and Zhu, J.J. (2002). Signaling of layer 1 and whisker-evoked Ca^{2+} and Na^+ action potentials in distal and terminal dendrites of rat neocortical pyramidal neurons in vitro and in vivo. *J. Neurosci.* 22, 6991–7005.
- Larkum, M.E., Zhu, J.J., and Sakmann, B. (1999). A new cellular mechanism for coupling inputs arriving at different cortical layers. *Nature* 398, 338–341.
- Larkum, M.E., Senn, W., and Lüscher, H.R. (2004). Top-down dendritic input increases the gain of layer 5 pyramidal neurons. *Cereb. Cortex* 14, 1059–1070.
- Larkum, M.E., Nevian, T., Sandler, M., Polsky, A., and Schiller, J. (2009). Synaptic integration in tuft dendrites of layer 5 pyramidal neurons: a new unifying principle. *Science* 325, 756–760.
- Losonczy, A., and Magee, J.C. (2006). Integrative properties of radial oblique dendrites in hippocampal CA1 pyramidal neurons. *Neuron* 50, 291–307.
- Losonczy, A., Makara, J.K., and Magee, J.C. (2008). Compartmentalized dendritic plasticity and input feature storage in neurons. *Nature* 452, 436–441.

- Matyas, F., Sreenivasan, V., Marbach, F., Wacongne, C., Barsy, B., Mateo, C., Aronoff, R., and Petersen, C.C. (2010). Motor control by sensory cortex. *Science* 330, 1240–1243.
- Nicoll, R.A., Malenka, R.C., and Kauer, J.A. (1990). Functional comparison of neurotransmitter receptor subtypes in mammalian central nervous system. *Physiol. Rev.* 70, 513–565.
- O'Connor, D.H., Peron, S.P., Huber, D., and Svoboda, K. (2010). Neural activity in barrel cortex underlying vibrissa-based object localization in mice. *Neuron* 67, 1048–1061.
- Oberlaender, M., de Kock, C.P., Bruno, R.M., Ramirez, A., Meyer, H.S., Dercksen, V.J., Helmstaedter, M., and Sakmann, B. (2012). Cell type-specific three-dimensional structure of thalamocortical circuits in a column of rat vibrissa cortex. *Cereb. Cortex* 22, 2375–2391.
- Petreaanu, L., Mao, T., Sternson, S.M., and Svoboda, K. (2009). The subcellular organization of neocortical excitatory connections. *Nature* 457, 1142–1145.
- Rall, W. (1964). Theoretical significance of dendritic trees for neuronal input-output relations. In *Neural Theory and Modeling*, R.F. Reiss, ed. (Palo Alto, CA: Stanford Univ. Press), pp. 73–94.
- Schaefer, A.T., Helmstaedter, M., Schmitt, A.C., Bar-Yehuda, D., Almog, M., Ben-Porat, H., Sakmann, B., and Korngreen, A. (2007). Dendritic voltage-gated K⁺ conductance gradient in pyramidal neurones of neocortical layer 5B from rats. *J. Physiol.* 579, 737–752.
- Schiller, J., Schiller, Y., Stuart, G., and Sakmann, B. (1997). Calcium action potentials restricted to distal apical dendrites of rat neocortical pyramidal neurons. *J. Physiol.* 505, 605–616.
- Schiller, J., Major, G., Koester, H.J., and Schiller, Y. (2000). NMDA spikes in basal dendrites of cortical pyramidal neurons. *Nature* 404, 285–289.
- Takahashi, H., and Magee, J.C. (2009). Pathway interactions and synaptic plasticity in the dendritic tuft regions of CA1 pyramidal neurons. *Neuron* 62, 102–111.
- Vetter, P., Roth, A., and Häusser, M. (2001). Propagation of action potentials in dendrites depends on dendritic morphology. *J. Neurophysiol.* 85, 926–937.
- Williams, S.R. (2004). Spatial compartmentalization and functional impact of conductance in pyramidal neurons. *Nat. Neurosci.* 7, 961–967.
- Williams, S.R. (2005). Encoding and decoding of dendritic excitation during active states in pyramidal neurons. *J. Neurosci.* 25, 5894–5902.
- Williams, S.R., and Stuart, G.J. (2002). Dependence of EPSP efficacy on synapse location in neocortical pyramidal neurons. *Science* 295, 1907–1910.
- Williams, S.R., and Atkinson, S.E. (2007). Pathway-specific use-dependent dynamics of excitatory synaptic transmission in rat intracortical circuits. *J. Physiol.* 585, 759–777.
- Wimmer, V.C., Bruno, R.M., de Kock, C.P., Kuner, T., and Sakmann, B. (2010). Dimensions of a projection column and architecture of VPM and POM axons in rat vibrissa cortex. *Cereb. Cortex* 20, 2265–2276.
- Xu, N.-L., Harnett, M.T., Williams, S.R., Huber, D., O'Connor, D.H., Svoboda, K., and Magee, J.C. (2012). Nonlinear dendritic integration of sensory and motor pathways produces an object localization signal. *Nature* 492, 247–251.
- Yue, L., Feng, J.L., Wang, Z., and Nattel, S. (2000). Effects of ambasilide, quinidine, flecainide and verapamil on ultra-rapid delayed rectifier potassium currents in canine atrial myocytes. *Cardiovasc. Res.* 46, 151–161.